Heliyon 10 (2024) e30345

Contents lists available at ScienceDirect

Heliyon

journal homepage: www.cell.com/heliyon

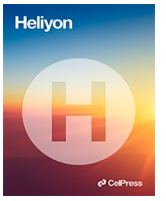

Research article

Efficient adsorption of rhodamine B using synthesized Mg–Al hydrotalcite/ sodium carboxymethylcellulose/ sodium alginate hydrogel spheres: Performance and mechanistic analysis

Siqi Chang [a], Xiangling Zhang [a,b,*], Chen Wang [a], Jing Bai [a], Xuhao Li [a], Wei Liang [a], Yajia Mao [a], Jixian Cai [a], Yifan Li [a,b], Yu Jiang [a], Zhouying Xu [a]

[a] School of Civil Engineering and Architecture, Wuhan University of Technology, Wuhan, 430070, China
[b] Sanya Science and Education Innovation Park, Wuhan University of Technology, Hainan, 572024, China

ARTICLE INFO

Keywords:
Sodium alginate
Carboxymethyl cellulose
Sodium dodecyl sulfate
Magnesium aluminum hydrotalcite
Rhodamine B

ABSTRACT

In this study, the sodium dodecyl sulfate intercalated modified magnesium-aluminum hydrotalcite/sodium alginate/sodium carboxymethylcellulose (modified LDHs/SA/CMC) composite gel spheres were synthesized and their efficacies in adsorbing the cationic dye rhodamine B (RhB) from aqueous solutions were evaluated. The effects of adsorption time, pH and temperature on the adsorption of RhB by spheres were investigated. Remarkably, the modified LDHs/SA/CMC gel spheres achieved adsorption equilibrium after 600 min at 25 °C, and the removal rate of RhB at 60 mg/L reached 91.49 % with the maximum adsorption capacity of 59.64 mg/g. The gel spheres maintained over 80 % efficacy across four adsorption cycles. Kinetic and isotherm analyses revealed that the adsorption of RhB conformed to the secondary kinetic model and the Langmuir isotherm, indicating a spontaneous and exothermic nature of the adsorption process. The adsorption mechanisms of modified LDHs/SA/CMC gel spheres on RhB dyes include electrostatic adsorption, hydrogen bonding and hydrophobic interactions. In conclusion, modified LDHs/SA/CMC gel sphere is a green, simple, recyclable and efficient adsorbent, which is expected to be widely used for the treatment of cationic dye wastewater.

1. Introduction

Rhodamine B (RhB), a synthetic red alkaline fluorescent dye from the triphenylmethane family, is extensively used as a colorant in the textile industry, favored for its high stability and resistance to biodegradation [1,2]. However, its carcinogenic and neurotoxic properties pose significant health risks, including respiratory infections, skin and gastrointestinal irritation, and damage to the liver and thyroid [3,4]. Consequently, the removal of RhB from water sources is a critical environmental challenge. Among the various dye removal strategies—such as physical adsorption [5], photocatalytic degradation [6], advanced oxidation processes [7], and microbial treatment [8], adsorption stands out as a promising method due to its simple design, ease of operation, low cost, low chemical requirements, and lack of inhibition by toxic substances [9,10].

Magnesium-aluminum hydrotalcite (MgAl-LDHs) is a type of layered bimetallic hydroxide [11], renowned for its unique layered

* Corresponding author. School of Civil Engineering and Architecture, Wuhan University of Technology, 122, Luoshi Road, Hongshan District, Wuhan, 430070, China.
E-mail address: ZXLCL@126.com (X. Zhang).

https://doi.org/10.1016/j.heliyon.2024.e30345
Received 12 April 2024; Received in revised form 23 April 2024; Accepted 24 April 2024
Available online 28 April 2024

structure and exchangeable interlayer anions, endowing it with a potent capability for pollutant removal from water, particularly anions [12]. The surface properties of LDHs can be modulated from hydrophilic to hydrophobic by employing surfactants or biomolecules as soft templates [13], thereby augmenting their proficiency in extracting organic pollutants from aqueous environments [14]. For instance, Qin et al. [15] utilized defect-ordered MgAl-LDHs nanosheets to adsorb the Congo red dye, achieving an impressive adsorption capacity of 262.4 mg/g; Chakraborty et al. [16] developed MgAl-LDHs loaded metal-organic framework nanocomposites, which exhibited a rapid adsorption of methyl orange (99 mg/g within 20 min). Despite these strengths, the use of LDHs in powdered form poses challenges such as proneness to agglomeration, difficult recovery, and potential secondary contamination, thus hindering their practical application. Integrating LDHs into sodium alginate (SA) gel spheres presents an innovative solution to these limitations [17], offering a more efficient and environmentally benign approach to water purification.

Alginate, a natural biopolymer sourced from brown algae, stands out for its non-toxicity, biodegradability, biocompatibility, and cost-effectiveness [18]. When processed into hydrogels, alginate's mechanical stability and durability can be significantly enhanced through physicochemical modifications [19,20]. These improvements are pivotal in augmenting its adsorption properties, particularly in increasing its capacity to adsorb pollutants [21]. The creation of hydrogel spheres has emerged as a prevalent technique to boost alginate's adsorptive capabilities [22]. However, poor mechanical strength and low rigidity limit the direct use of sodium alginate as an adsorbent application [23], the combination with organic matter can improve the mechanical properties and stability of the gel, and increase the functional groups and effective adsorption sites of the adsorbent [24]. Hence, the integration of alternative adsorbent materials within sodium alginate matrices is critical for optimizing the adsorption capacity and efficiency. Carboxymethyl cellulose (CMC), an anionic, water-soluble cellulose derivative, is renowned for its renewable and biodegradable nature. It can be crosslinked with multivalent metal cations to form solid gels with a stabilized three-dimensional mesh structure [25]. Both SA (sodium alginate) and CMC are natural polymers characterized by excellent biodegradability and compatibility. Rich in –OH and –COOH groups, they exhibit a strong affinity for pollutant molecules, enabling rapid removal of contaminants from wastewater via mechanisms such as electrostatic adsorption, ion exchange, and hydrogen bonding [26]. Chen et al. [27] synthesized magnetic SA/CMC interpenetrating network gel spheres capable of adsorbing dyes DV51 and DR23 at capacities of up to 2782 mg/g and 2868 mg/g, respectively, in neutral environments. Similarly, Ren et al. [28] developed SA CMC gel pellets which demonstrated a remarkable Pb^{2+} adsorption capacity, reaching up to 1.73 g/g. These examples underscore the potential of SA and CMC-based materials in high-efficiency pollutant adsorption, making valuable in wastewater treatment applications.

In this research, novel gel spheres composed of modified layered double hydroxides (LDHs), sodium alginate (SA), and sodium carboxymethyl cellulose (CMC) were synthesized using sodium dodecyl sulfate-modified magnesium-aluminum hydrotalcite as the embedding material and calcium chloride as the cross-linker. These gel spheres, abundant in functional groups, were specifically engineered for the effective adsorption of RhB dyes. The primary aims of this study were to delineate the material's morphology and structure, assess its capacity for RhB removal, and elucidate the underlying mechanisms of RhB adsorption. The findings revealed that these gel spheres exhibit significant adsorption efficiency for RhB, characterized by ease of operation, straightforward recovery, and robust reusability. These attributes earmark the modified LDHs/SA/CMC gel spheres as a promising solution for dye wastewater treatment, offering practical and sustainable remediation avenues.

2. Experimental materials and methods

2.1. Materials

Sodium alginate (SA), sodium carboxymethyl cellulose (CMC), $Mg(NO_3)_2{\bullet}6H_2O$, $Al(NO_3)_3{\bullet}9H_2O$, NaOH, Na_2CO_3, sodium dodecahydrate sulfate(SDS), $CaCl_2$ were purchased from Sinopharm Group, and the water used in the experiments was deionized.

2.2. Synthesis of composite gel spheres

2.2.1. Synthesis of modified MgAl-LDHs

Modified magnesium aluminum-layered double hydroxides (MgAl-LDHs) were synthesized through the co-precipitation technique. Magnesium nitrate hexahydrate ($Mg(NO_3)_2{\bullet}6H_2O$) and aluminum nitrate nonahydrate ($Al(NO_3)_3{\bullet}9H_2O$) were solubilized in 250 mL of deionized water. Concurrently, a 0.1 mol sodium dodecyl sulfate (SDS) solution (50 mL) was introduced into the aqueous metal salt mixture. The pH was meticulously regulated to a range of 8–9 using a sodium hydroxide and sodium carbonate solution. The system was subsequently subjected to continuous stirring at 75 °C for 2 h. Following this, the resultant slurry underwent an aging process at 70 °C for an additional 24 h. The material was then isolated by filtration, rinsed to neutrality, and desiccated at 70 °C.

2.2.2. Synthesis of modified LDHs/SA/CMC gel spheres

Composite layered double hydroxides (LDHs) incorporating sodium alginate and sodium carboxymethyl cellulose were formulated via a meticulous procedure (Fig. S1). The constituents were dissolved in deionized water at 60 °C, employing a stoichiometric mass ratio of 2:1:2. Subsequently, the mixture was subjected to ultrasonic agitation for 30 min to ensure homogeneity. After a defoaming period, the aqueous composition was incrementally introduced into a 2 % mass fraction calcium chloride ($CaCl_2$) solution using a precision syringe. This facilitated the cross-linking process, which was carried out over a 12-h interval. The emergent gel spheres were isolated, rigorously rinsed with deionized water 3–4 times to eliminate residual reactants, and finally desiccated in vacuum drying oven at 60 °C for 2 h. The loading of modified LDHs was calculated on basis of the average mass of the material after three preparations. The mass of the material preparation stage was 2.5000 g, and the mass of the dried gel pellet after preparation was 2.7205 g, which

gave a content of modified LDHs of about 36.76 %.

2.3. Characterization

The comprehensive characterization of the materials involved multiple sophisticated analytical techniques. X-ray diffraction (XRD, Empyrean, Netherlands) was employed to elucidate the crystal structure, providing insights into the lattice arrangements and phase compositions. Fourier transform infrared spectrometry (FT-IR, Nicolet 6700, USA), spanning a range of 400 cm^{-1} to 4000 cm^{-1}, was utilized to capture the infrared spectra of the samples, offering details about the functional groups and molecular interactions. The microstructural features of the materials were meticulously examined using scanning electron microscopy (SEM, Zeiss Ultra Plus, Germany), which allowed for a detailed visualization of surface morphology and particle size. Finally, X-ray photoelectron spectroscopy (XPS, Thermo Kalpha, USA) was conducted to analyze the elemental composition and valence states within the materials, thereby shedding light on their chemical environment and electronic structure. These combined analytical approaches provided a holistic understanding of the materials' properties and potential functionalities.

2.4. Adsorption experiments

To assess the adsorption capacity of the modified LDHs/SA/CMC composite gel spheres for RhB, a 100 mL RhB solution at a concentration of 60 mg/L was prepared. The pH of this solution was adjusted from 3 to 11 using 0.1 mol/L HCl and NaOH. Subsequently, a series of dosages (25, 50, 100, 200, 300, 400, 500, 600 mg) of composite gel spheres were introduced into the solution. The adsorption process was conducted in a thermostatic oscillator at room temperatur. After 600 min of adsorption, the supernatants were transferred to a centrifuge tube using a 5 mL pipette gun, and the absorbance of the solutions was measured at 554 nm using a UV spectrophotometer after centrifugation. Each type of experiment included a blank group (without adsorbent) and was repeated three times, and the average absorbance of the results of the three groups of experiments was taken as the final value for graphing and fitting, and the adsorption amount and removal rate were calculated, with the standard deviation as the value of the error bar. The formulae are shown below:

$$q_e = \frac{(C_0 - C_e)V}{\mathrm{m}} \tag{1}$$

where: q_e is the equilibrium adsorption amount at adsorption equilibrium (mg/g).

C_0 is the RhB ion concentration in the initial solution (mg/L);
C_e is the RhB ion concentration in the solution at adsorption equilibrium (mg/L);
V is the volume of the solution (L);
m is the mass of the gel sphere (g).

Removal rate calculation formula:

$$E = \frac{(C_0 - C_e)}{C_0} \times 100\% \tag{2}$$

where: E is the removal rate (%) at adsorption equilibrium; C_0 is the RhB concentration in the initial solution (mg/L); C_e is the RhB concentration in the solution at adsorption equilibrium (mg/L).

2.5. Adsorption isotherm studies

The Langmuir (Eq. (3)), Freundlich (Eq. (4)), Temkin (Eq. (5)), and Sips (Eq. (6)) model was used to fit the behavior of RhB adsorption on modified LDHs/SA/CMC gel spheres.

$$q_e = \frac{q_m K_L C_e}{1 + K_L C_e} \tag{3}$$

$$q_e = K_F \cdot C_e^{\frac{1}{n}} \tag{4}$$

$$q_e = \frac{RT}{b} \ln(C_e) + \frac{RT}{b} \ln(K_T) \tag{5}$$

$$q_e = \frac{q_m (K_s C_e)^m}{1 + (K_s C_e)^m} \tag{6}$$

where: q_m is the theoretical maximum adsorption amount (mg/g), C_e is the RhB concentration in the solution at adsorption equilibrium (mg/L), n is a measure of the linear deviation of the adsorption process, b is Temkin constant (J/mol), related to the heat of adsorption, R is the molar gas constant (8.314 J/K·mol). K_L, K_F, K_T, and K_S are the adsorption constants of the Langmuir, Freundlich, Temkin, and

Sips models, respectively.

2.6. Adsorption kinetic

The kinetic adsorption results were fitted using the pseudo-first-order kinetic model (Eq. (7)), the pseudo-second-order kinetic model (Eq. (8)), and the intra-particle diffusion model (Eq. (9)).

$$\frac{q_t}{q_e} = 1 - e^{-k_1 t} \tag{7}$$

$$\frac{q_t}{q_e} = \frac{k_2 q_e t}{1 + k_2 q_e t} \tag{8}$$

$$q_t = k_i t^{1/2} + c_i \tag{9}$$

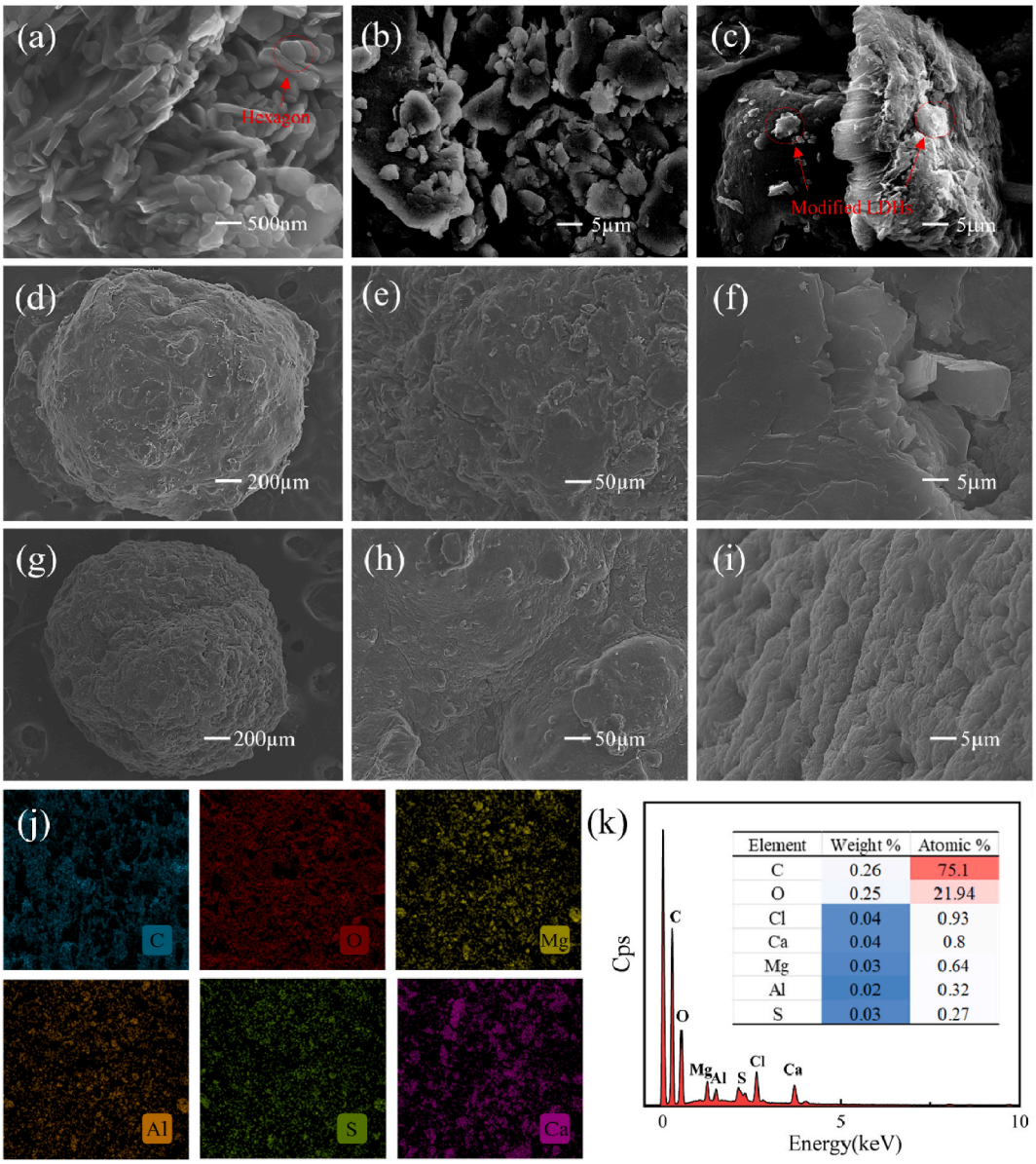

Fig. 1. (a)–(c) SEM images of MgAl-LDHs, modified LDHs, and the grinding modified LDHs/SA/CMC gel spheres; (d)–(f) SEM images of modified LDHs/SA gel spheres; (g)–(i) SEM images and(j)-(k) EDS images of modified LDHs/SA/CMC gel spheres.

$$AARD_F = \frac{1}{N}\sum_{i=1}^{N}\left|\frac{\widehat{y_i} - y_i}{y_i}\right| \tag{10}$$

where: q_e is the equilibrium adsorption amount of gel spheres at equilibrium (mg/g); q_t is the adsorption amount at the moment t (mg/g); k_1 (min^{-1}) and k_2 (g/mg·min) are the coefficients of the pseudo-first-order and pseudo-second-order kinetic equations. k_i is the rate constant for intra-particle diffusion (mg·$min^{0.5}$/g); t is the reaction time (min): c_i is the boundary layer thickness. $AARD_F$ is the average absolute relative deviation (%).

2.7. Adsorption thermodynamics

The thermodynamic study of RhB adsorption on modified LDHs/SA/CMC gel spheres was carried out at 298.15 K, 308.15 K, and 318.15 K. The thermodynamic parameters of adsorption were calculated as shown below:

$$\Delta G = -RTLnK_{ML} \tag{11}$$

$$Ln\ K_{ML} = \frac{\Delta S}{R} - \frac{\Delta H}{RT} \tag{12}$$

$$\frac{C_e}{q_e} = \frac{C_s}{K_{ML}q_m} + \frac{(K_{ML}-1)C_e}{K_{ML}q_m} \tag{13}$$

where: q_e is the equilibrium adsorption amount at adsorption equilibrium (mg/g); C_e is the concentration of RhB in solution at adsorption equilibrium (mg/L); R is the universal gas constant (J/mol•K); T is the temperature (K); ΔH is the enthalpy change (kJ/mol); ΔS is the entropy change (kJ/mol•K); ΔG is the Gibbs free energy (kJ/mol). K_{ML} was obtained by fitting Eq. (13) [29], which is an acausal parameter that meets the IUPAC requirement that the equilibrium constant used to estimate ΔG should be acausal. C_s is the saturated concentration of RhB in aqueous solution (0.025 mol/L).

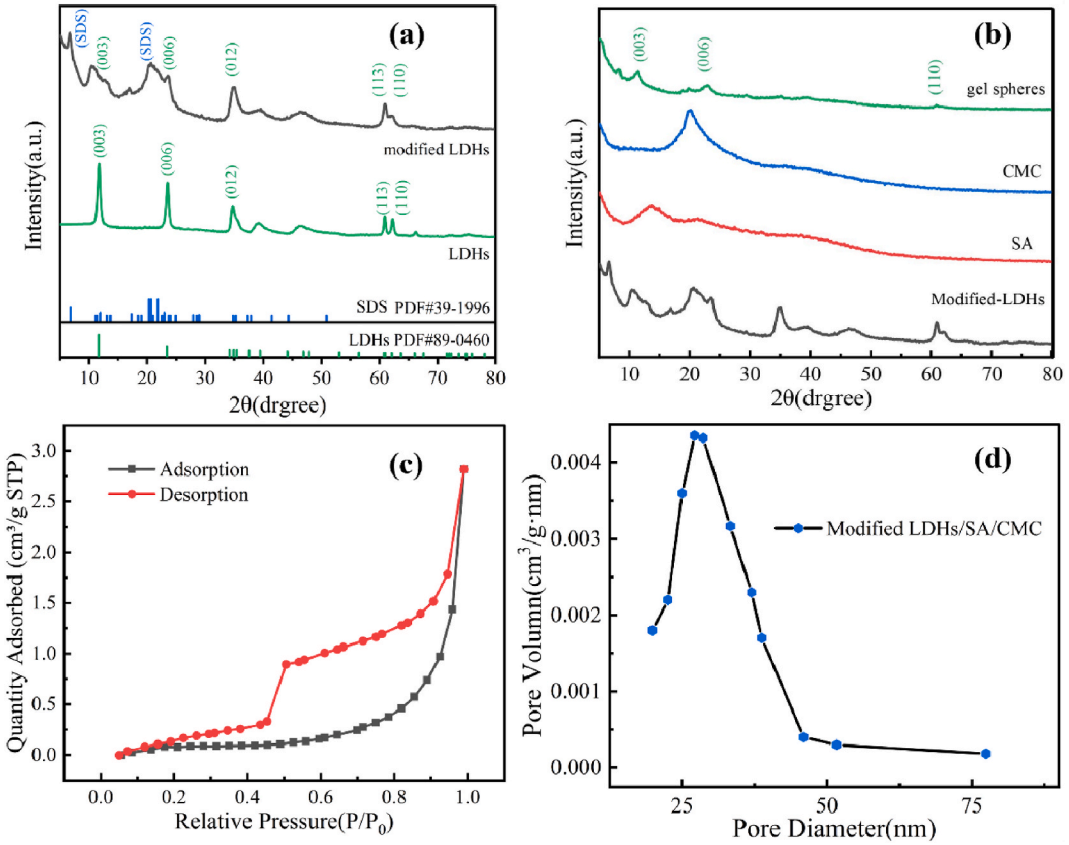

Fig. 2. (a–b) XRD patterns of MgAl-LDHs, modified LDHs, SA, CMC, and modified LDHs/SA/CMC gel spheres; (c) Adsorption-desorption isotherm of modified LDHs/SA/CMC gel spheres; (d) Pore size distribution of modified LDHs/SA/CMC gel spheres.

2.8. Desorption and regeneration experiment

At the end of the adsorption experiments, the gel spheres were separated from the solution, washed with deionized water, placed in a conical flask containing 100 mL of the ethanol desorption solution, shaken in a shaker at 160 rpm for 12 h at 298.15 K, and then separated, dried, and reused. Following this procedure, the adsorption experiments were repeated four times.

3. Results and discussion

3.1. Characterization of the adsorbents

As shown in Fig. 1a and b, the MgAl-LDHs showed a stacked classical hexagonal and lamellar structural morphology on the microscopic scale [30]. Upon composite with SDS, the modified LDHs showed a stacked plate-like structure with blunted boundaries on the microscopic scale. As can be seen in Fig. 1c, the modified LDHs were distributed on the cross-section of the gel spheres, which implies the successful preparation of the composite gel spheres. In Fig. 1d and g, at a 200 μm resolution, the composite gel material appeared as spherical entities with an average diameter of around 1–2 mm, characterized by a rough surface texture. Higher resolution images at 50 μm and 5 μm revealed a series of irregular folds on the gel spheres' surface, likely due to the partial collapse of the polymer network during the drying and dehydration phases [31,32]. Further observation revealed that the surface of the CMC-added gel spheres is rougher due to the condensation reaction between the carboxyl group of SA and the hydroxyl group of CMC, which released heat and promoted the formation of a mesh structure through thermal expansion [33], thus increasing the roughness and specific surface area.

The EDS data in Fig. 1k indicated that the modified LDHs/SA/CMC gel spheres comprise significant amounts of Mg, Al, and S. The atomic ratio of Mg to Al was approximately 2:1 (0.64:0.32), suggesting the successful integration of modified MgAl-LDHs into the SA/CMC matrix. Furthermore, the EDS spectra in Fig. 1j demonstrated a uniform elemental distribution in the prepared gel spheres, with no evidence of segregation, thereby confirming the effective synthesis of these composite gel spheres.

In Fig. 2a–b, the XRD patterns of modified LDHs, SA, CMC, and modified LDHs/SA/CMC gel spheres were presented. Fig. 2a revealed that the synthesized MgAl-LDHs samples exhibit sharp, well-defined peaks characteristic of hydrotalcite-like compounds, signifying a well-structured layered crystal formation [34–36]. Upon integration with SDS, as observed in Fig. 2a, the original LDHs characteristic peaks were accompanied by distinct, symmetric diffraction peaks of SDS (JCPDS card no. 39–1996) at $2\theta = 6.8^\circ$ and 20.5°, and around $2\theta = 11^\circ$, the (003) crystal plane of LDHs forms a new crystal plane together with the SDS plane. This indicated that SDS aggregates on the LDHs' surface, affecting its crystallinity [18]. In Fig. 2b, the XRD patterns of the modified LDHs/SA/CMC gel spheres, juxtaposed with those of SA and CMC, exhibited distinct peaks at 2θ values of 11.65°, 23.62°, and 60.76°. However, these peaks were notably diminished in intensity, a phenomenon attributed to the decreased crystallinity resulting from the composite formation of SA and CMC. This attenuation of peak intensity also confirmed the successful integration of modified LDHs with SA and CMC, signaling the formation of a new composite material with distinctly modified structural attributes.

Fig. 2c and d showcased the adsorption-desorption isotherms and pore size distributions of modified LDHs/SA/CMC gel spheres, respectively. As shown in Fig. 2c, the adsorption-desorption curves of the gel spheres showed iv-type isotherms according to the IUPAC classification, and h3-type hysteresis lines were observed [37]. As can be seen from Fig. 2d, the pore size distribution of the spheres was not uniform and was mainly dominated by mesopores, with the pore size concentrated at 27.12 nm. In addition, the spheres also have some large pores, and the appropriate pore size and pore volume were favorable for the adsorption of RhB dyes with a molecular size of

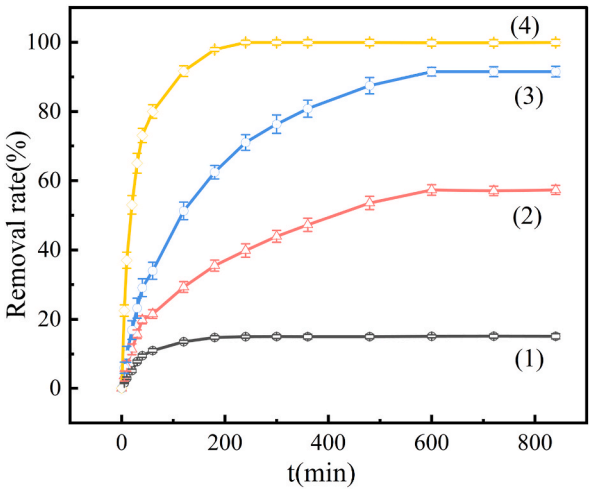

Fig. 3. Adsorption curves of (1) SA/CMC gel spheres, (2) modified LDHs/SA gel spheres, (3) modified LDHs/SA/CMC gel spheres, (4) modified LDHs.

15.9 Å × 11.8 Å × 5.6 Å [38].

3.2. Verification and comparison of adsorption performance

Fig. 3 presented the adsorption profiles of four distinct materials on RhB, under specific conditions: RhB concentration at 60 mg/L and an adsorbent dosage of 0.2 g. The materials' adsorption capacities for RhB were arrayed in descending order: modified LDHs demonstrated the highest adsorption, succeeded by modified LDHs/SA/CMC gel pellets, modified LDHs/SA gel pellets, and finally, SA/CMC gel pellets, which exhibited the lowest adsorption. The modified LDHs were notably the most efficacious in adsorbing RhB. However, their integration into gel spheres led to a discernible dip in adsorption efficiency, a result that was in line with initial expectations. This phenomenon was partially elucidated by observations in Fig. 3, where SA/CMC gel pellets alone managed only about a 15 % removal rate, highlighting their restricted adsorptive capacity. Consequently, the amalgamation of SA/CMC with modified LDHs diminished the latter's overall adsorptive effectiveness. Additionally, the gel spheres' surface area significantly reduced compared to the powdered form of modified LDHs, further contributing to the decline in adsorption efficiency. This analysis effectively highlighted how the composition and structural characteristics of materials can substantially influence their adsorption capabilities. The addition of carboxymethyl cellulose (CMC) to the modified LDHs/SA gel spheres, forming the modified LDHs/SA/CMC composite, markedly enhanced the RhB removal rate, increasing it from 57 % to 91 %. The increase in adsorption performance was consistent with the results obtained from SEM analysis and additionally suggested that binding with CMC can increase the functional groups and effective adsorption sites of SA gel adsorbents.

3.3. Effect of dosage on adsorption

Fig. 4a illustrated the relationship between the dosage of modified LDHs/SA/CMC gel spheres and their efficacy in removing and adsorbing RhB. The analysis showed a gradual decrease in the adsorption amount of RhB with increasing dosages of the gel spheres, ranging from 25 mg to 600 mg, while the removal rate experienced a significant enhancement. Notably, at a gel sphere dosage of 400 mg, the RhB removal rate reached a stable plateau. The number of available adsorption sites increased with the increase in adsorbent dosage and hence the removal of RhB increased, reaching 97.63 % at 400 mg. In addition, the increase of adsorption sites led to an increase in the competition for RhB molecules, and not every adsorption site could effectively capture RhB molecules [39], and thus its

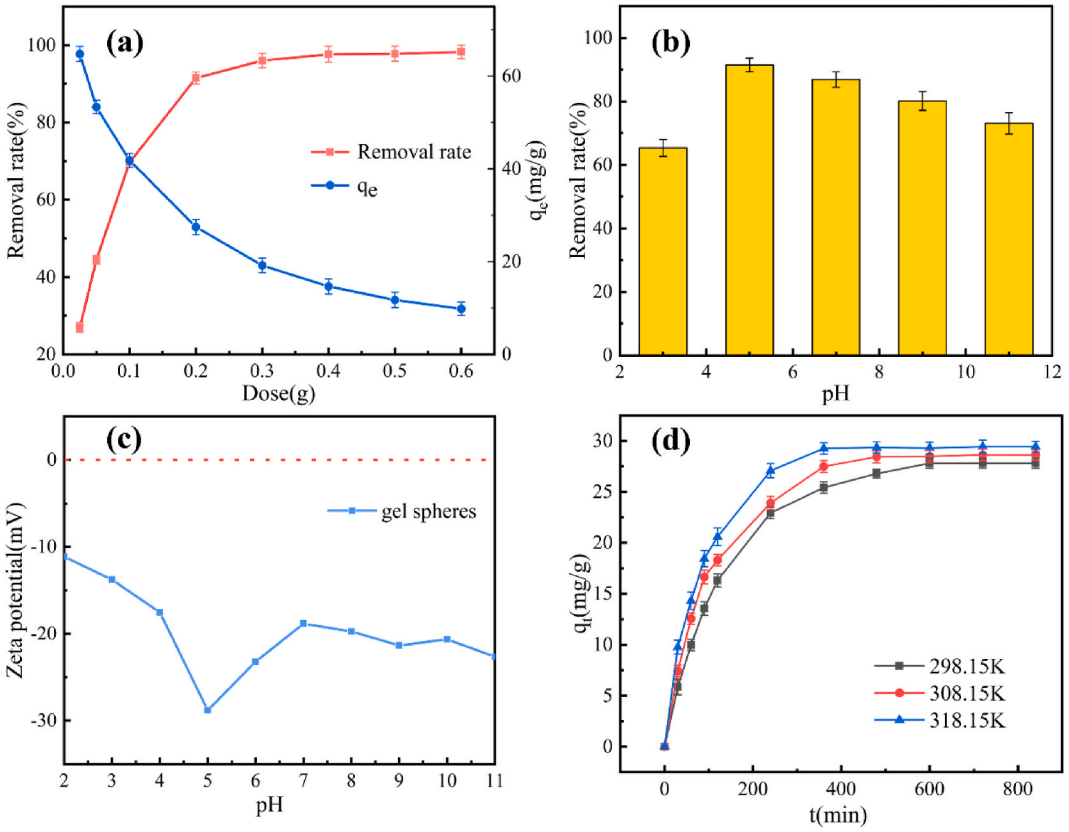

Fig. 4. (a) Effect of adsorbent dosage on adsorption; (b) Effect of pH on adsorption; (c) Zeta potential of modified LDHs/SA/CMC gel spheres; (d) Effect of temperature on adsorption.

adsorption capacity was decreasing.

3.4. Effect of pH on adsorption

Fig. 4b delineated the interplay between solution pH and the removal and adsorption of RhB. The figure demonstrated that solution pH markedly influenced RhB adsorption, with both the removal rate and adsorption amount of RhB by the gel spheres progressively increasing as the pH rose from 3 to 5. Optimal RhB removal, reaching 91.49 %, occurred at pH 5. This efficacy could be attributed to the higher concentration of H^+ ions at lower pH levels, leading to the protonation of functional groups on the gel spheres' surface. These protonated groups, being positively charged, repelled the similarly charged RhB molecules, resulting in reduced electrostatic attraction and, consequently, lower adsorption.

As the pH continued to increase from 5 to 11, the removal rate and adsorption amount of RhB by the gel spheres began to decline, dropping to 73.09 % at pH 11. This decline is likely because RhB assumes an amphoteric ion form in water at pH levels above 4, diminishing the interaction between the negatively charged membrane surface and the RhB dye [40]. To substantiate the pH effect on RhB adsorption, the zeta potential of the gel spheres was analyzed. As shown in Fig. 4c, the zeta potential of the modified LDHs/SA/CMC gel spheres remained negative across a pH range of 2–11, reaching a peak negative charge at pH 5 with a potential of −28.8 mV. Concurrently, the RhB dye in the solution was positively charged, aligning with the experimental observations. Consequently, pH 5 was identified as the optimal condition for adsorption experiments, setting the stage for all subsequent experiments to be conducted at this pH level.

3.5. Effect of temperature on adsorption

Fig. 4d exhibited the adsorption capacity of modified LDHs/SA/CMC gel spheres for RhB at reaction temperatures of 298.15 K, 308.15 K, and 318.15 K. As depicted in Fig. 4d, the equilibrium adsorption capacity of RhB by the gel spheres was 27.44 mg/g at 298.15 K, corresponding to a removal rate of 91.49 %. Intriguingly, this capacity enhanced progressively with increasing temperature. At 308.15 K and 318.15 K, the equilibrium adsorption capacities were 28.62 mg/g and 29.43 mg/g, respectively. As can be seen from Table 1, a positive ΔH value indicated that the adsorption process was endothermic, with rising temperatures favoring the adsorption and thus increasing RhB uptake from water. The negative ΔG values suggested that RhB adsorption by the gel spheres was a spontaneous process. Furthermore, a positive ΔS value implied an increase in disorder at the solid-liquid interface during RhB adsorption, signifying a state of increased entropy.

3.6. Adsorption kinetic studies

Fig. 5a and b depicted the fitted curves for the pseudo-first-order and pseudo-second-order kinetic models, with the corresponding parameters detailed in Table 2. Analysis of this data revealed that the linear correlation coefficient R^2 for the pseudo-second-order kinetic model (0.9947) exceeded that of the pseudo-first-order model (0.9880), and its $AARD_{F2}$ is also smaller (8.16 %). In addition, the R^2 of both is greater than 0.8 and the residuals are randomly distributed around zero, so it can be assumed that the kinetic model was successfully fitted [41] and the adsorption of RhB on modified LDHs/SA/CMC gel spheres more accurately fits the pseudo-second-order kinetic model [42]. This observation tentatively suggests that chemisorption may be the main driver of the adsorption process [43], although the specific adsorption mechanism still requires further analysis.

In Fig. 5c, the fitted curves for the intraparticle diffusion model were showcased, with the relevant parameters enumerated in Table 3. Analysis of Fig. 5c and Table 3 revealed that the RhB adsorption process on the modified LDHs/SA/CMC gel spheres encompassed three distinct phases. Initially, the first phase was characterized by the diffusion of RhB from the solution to the surface of the gel spheres, exhibiting a steeper slope in the curve. This was attributed to the abundance of carboxyl and hydroxyl groups on the surface of the gel spheres, which provided a plethora of active adsorption sites for RhB, rendering surface adsorption the dominant mechanism at this early stage [44]. Subsequently, the second phase involved the diffusion of RhB into the pores of the adsorbent [45]. As the surface adsorption sites became increasingly occupied, a concentration gradient of RhB developed between the surface and the internal cavities of the gel spheres, prompting RhB to diffuse towards the inner surfaces. The final phase represented the equilibrium stage between adsorption and desorption [19]. Here, the adsorption sites on the gel spheres were fully occupied, leading to a saturation of the adsorption capacity. This stage marked the point at which the adsorption process stabilized, reflecting a balance between the uptake and release of RhB molecules.

Table 1
Parameters related to adsorption thermodynamics of RhB on modified LDHs/SA/CMC gel spheres.

T/K	LnK_{ML}	ΔG (kJ/mol)	ΔS (kJ/mol·K)	ΔH (kJ/mol)
298.15	8.427	−20.889	0.439	110.162
308.15	9.869	−25.285		
318.15	11.221	−29.680		

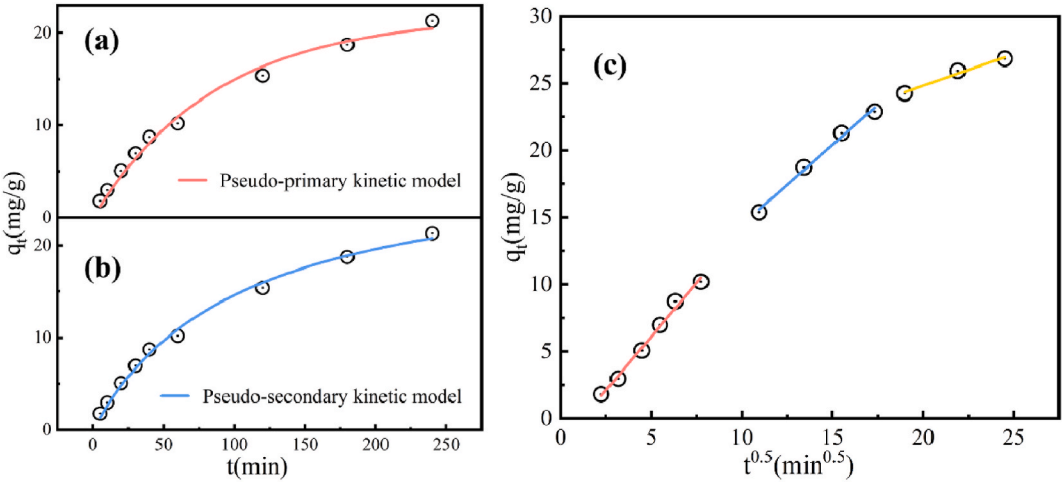

Fig. 5. (a) Pseudo-primary kinetic model (b) Pseudo-secondary kinetic model (c) Particle internal diffusion model (Adsorbent dosage: 0.2g, temperature: 25 °C, pH = 5, concentration of RhB: 60 mg/L).

Table 2
Fitted parameters for adsorption kinetics of RhB on modified LDHs/SA/CMC gel spheres.

Pseudo-first-order kinetic model				Pseudo-second-order kinetic model			
q_e (mg/g)	k_1 (min^{-1})	AARD$_{F1}$	R^2	q_e (mg/g)	k_2 (g/mg·min)	AARD$_{F2}$	R^2
21.85	0.0115	13.19	0.9880	29.77	3.22×10^{-4}	8.16	0.9947

Table 3
Fitting parameters of the intra-particle diffusion model for RhB adsorption by modified LDHs/SA/CMC gel spheres.

k_1 (mg·min$^{0.5}$/g)	R_1^2	k_2 (mg·min$^{0.5}$/g)	R_2^2	k_3 (mg·min$^{0.5}$/g)	R_3^2
1.60	0.9918	1.19	0.9922	0.47	0.9813

3.7. Adsorption isotherm studies

Fig. 6a to d displayed the Langmuir and Freundlich adsorption isotherm fitting curves for RhB adsorption onto modified LDHs/SA/CMC gel spheres. The corresponding isotherm parameters and correlation coefficients were tabulated in Table 4. Analysis revealed that the order of the average R^2 values for various models was Langmuir > Sips > Freundlich > Temkin. Analysis revealed that the Langmuir adsorption isotherm model, with a correlation coefficient (R^2) of 0.9984, exhibited a superior fit. This indicated that the adsorption of RhB onto the modified LDHs/SA/CMC gel spheres was predominantly characterized by monolayer adsorption [18], without significant interaction among the adsorbed RhB molecules [28].

At a constant temperature of 298 K, the theoretical maximum adsorption capacity was established at 59.64 mg/g. This suggested that the theoretical saturation adsorption capacity for the modified LDHs/SA/CMC gel spheres surpassed the maximum capacity observed in practical experiments. Furthermore, the Freundlich isotherm's n values, which were within the range of 1–10 (Table 4), underscored the efficacy of the modified LDHs/SA/CMC gel spheres as robust adsorbents [18]. The Temkin model relatively adequately described the RhB adsorption process ($R^2 = 0.9332$), indicating the non-uniformity of the spheres' surface and the weak interactions, such as electrostatic attraction between RhB and the gel spheres. The $q_{m,cal}$ of the Sips model was very close to the Langmuir model and the R^2(0.9981) is the second, which suggested that the adsorption of RhB dyes on gel spheres is mainly influenced by heterogeneous adsorption sites [46]. However, the main limitation of the Sips models is the lack of physical meaning of its parameters [47]. This affects the understanding of the adsorption process and mechanism. This comprehensive analysis affirmed their utility in the adsorptive removal of RhB, highlighting their potential in water treatment applications.

3.8. Adsorption mechanism

To investigate the interaction between modified LDHs/SA/CMC gel spheres and RhB dye, the FT-IR spectra of modified LDHs/SA/CMC gel spheres and synthesized materials (Fig. 7a) were obtained, as well as gel spheres before and after adsorption of RhB dye (Fig. 7b). As shown in Fig. 7a, the characteristic peaks due to the stretching vibration of –OH appeared at 3488 cm^{-1}, 3427 cm^{-1}, and 3435 cm^{-1} for modified LDHs, SA, and CMC, respectively [48,49], and the hydroxyl vibration appeared to partially overlap and the

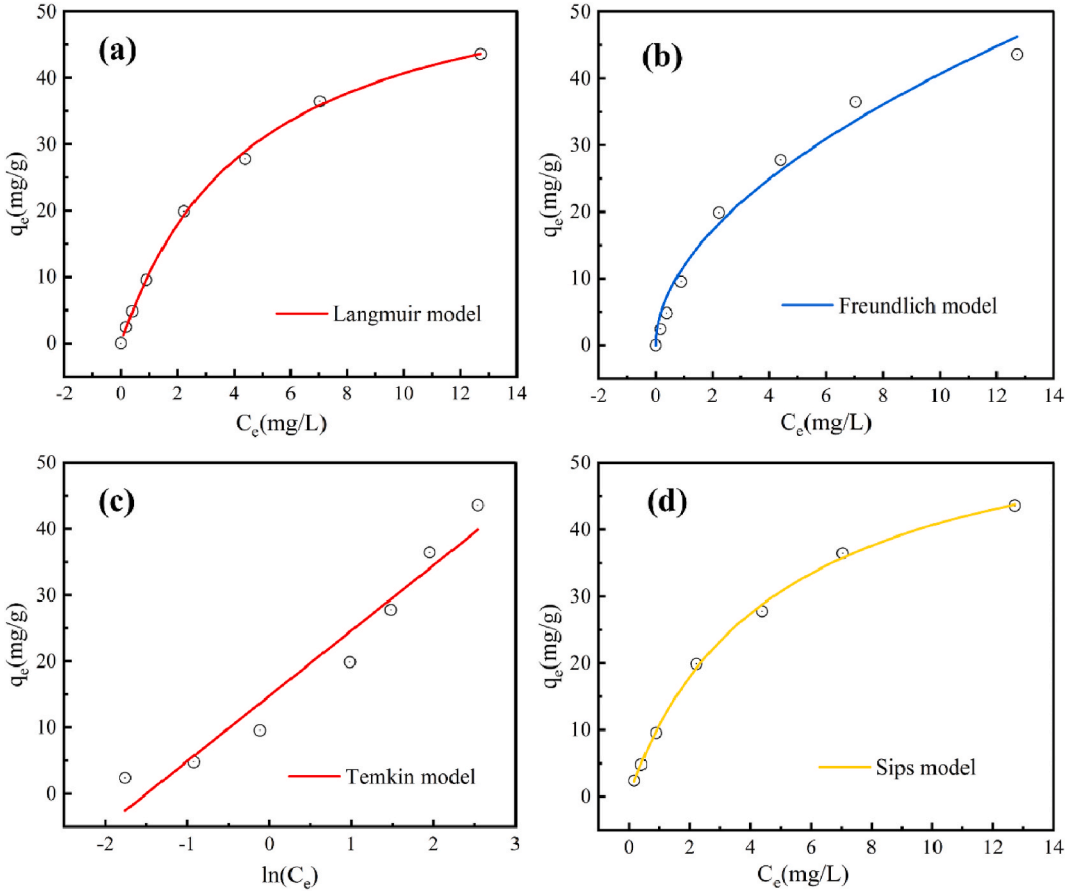

Fig. 6. Langmuir (a), Freundlich (b), Temkin (c), and Sips (d) isotherm models for the adsorption of RhB on modified LDHs/SA/CMC gel spheres (Adsorbent dosage: 0.2g, temperature: 25 °C, pH = 5, adsorption time: 600min).

Table 4
Adsorption parameters for RhB adsorption on modified LDHs/SA/CMC gel spheres.

Isotherm model	Parameters	
Langmuir isotherm	q_m **(mg/g)**	59.64
	K_L	0.215
	R^2	0.9984
Freundlich isotherm	n	1.870
	K_F	11.871
	R^2	0.9796
Temkin isotherm	b **(J/mol)**	251.168
	K_T	4.477
	R^2	0.9332
Sips isotherm	q_m **(mg/g)**	61.81
	m	0.964
	K_S	0.198
	R^2	0.9981

peaks were red-shifted from 3488 cm^{-1} to 3451 cm^{-1} after the composite of the modified LDHs and the gel spheres; and the vibrational peaks appeared near 2910-2930 cm^{-1} belonged to a series of characteristic peaks of methyl groups [32]. In addition, the modified LDHs/SA/CMC gel spheres were symmetric and asymmetric telescopic vibrations of –C═O at 1642 cm^{-1} versus 1471 cm^{-1} [27], which showed a blue-shift of the –C═O absorption peaks compared to that of the modified LDHs at 1634 cm^{-1} versus 1469 cm^{-1}. These spectral changes provided valuable insights into the molecular structure and interactions within the composite material upon RhB adsorption.

Upon the adsorption of RhB, as shown in Fig. 7b, notable alterations were observed in the positions and intensities of the major stretching vibration peaks of the modified LDHs/SA/CMC gel spheres. Specifically, the symmetric stretching vibration peaks of methyl,

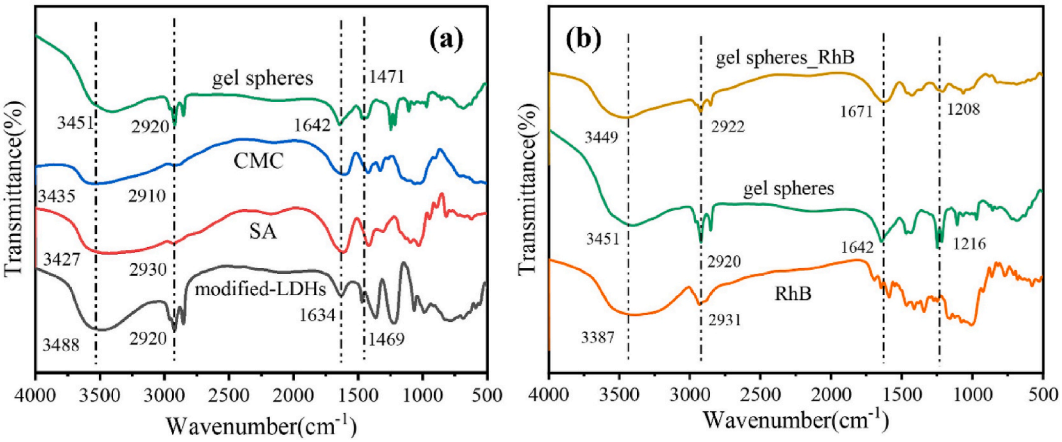

Fig. 7. (a)FT-IR spectra of modified LDHs, SA, CMC, and gel spheres; (b) FT-IR spectra of RhB, gel spheres before and after adsorption of RhB.

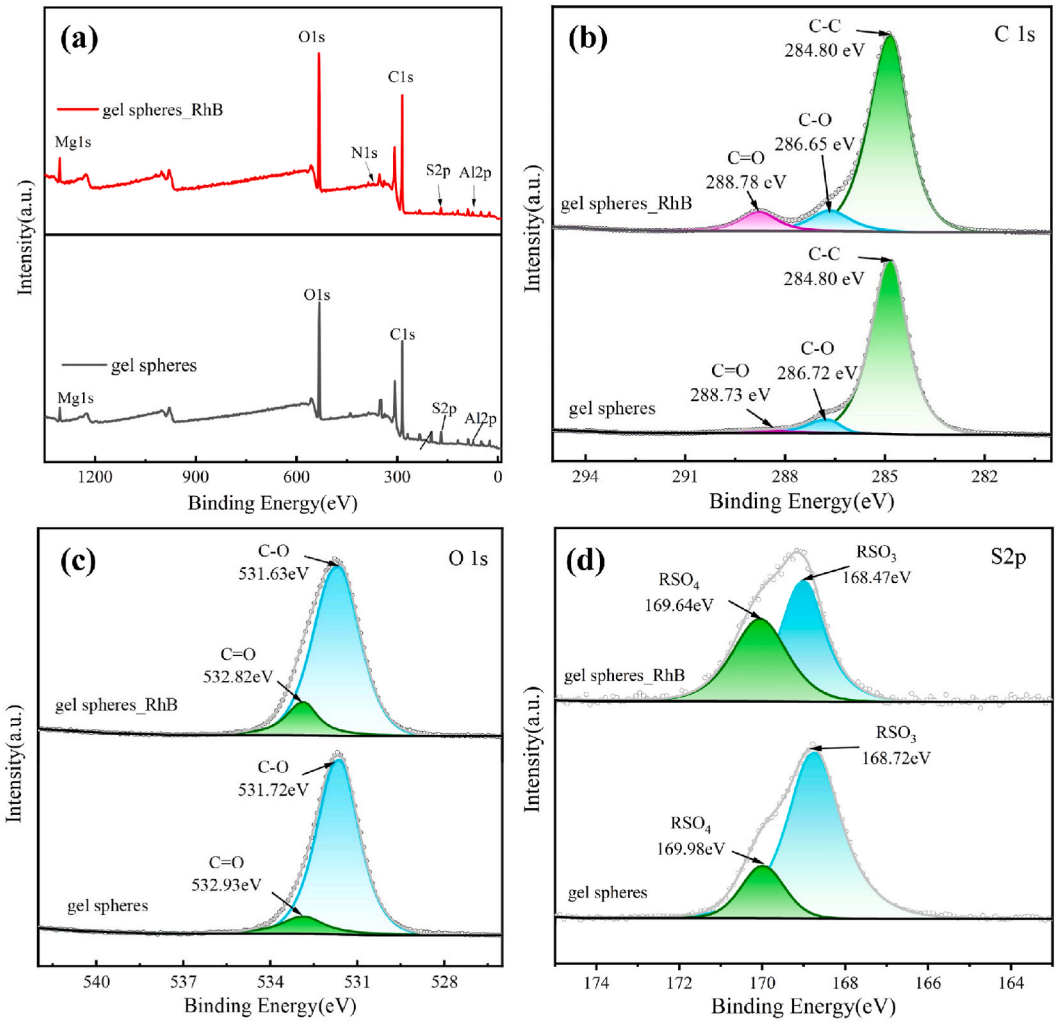

Fig. 8. (a) XPS survey spectra of modified LDHs/SA/CMC gel spheres; (b) high-resolution spectra of C1s; (c) high-resolution spectra of O1s; (d) high-resolution spectra of S2p.

hydroxyl (-OH), and carbonyl (-C═O) groups shifted from 3451 cm^{-1}, 2920 cm^{-1}, and 1642 cm^{-1} to 3449 cm^{-1}, 2922 cm^{-1}, and 1671 cm^{-1}, respectively. Remarkably, the stretching vibrational band of the S═O bond exhibited a blue shift from 1216 to 1208 cm^{-1} post-RhB adsorption, suggesting the occurrence of hydrophobic interactions between the modified LDHs in the spheres and the dye molecules [50]. These spectral changes are indicative of the involvement of chemical and hydrogen bonding interactions, particularly those involving hydroxyl and carboxyl groups, in the adsorption process between the modified LDHs/SA/CMC gel spheres and the RhB dye molecules. Such insights highlight the complex interplay of molecular forces during the adsorption process, underscoring the multifaceted nature of the interaction between the adsorbent and the adsorbate.

The interaction between RhB and modified LDHs/SA/CMC gel spheres was further scrutinized using X-ray photoelectron spectroscopy (XPS), as depicted in Fig. 8a. The comparative analysis of XPS spectra, before and after RhB adsorption, revealed the presence of nitrogen, a constituent of RhB, in the gel spheres post-adsorption, in addition to the standard elemental components. This finding confirmed the adsorption of RhB onto the surface of the modified LDHs/SA/CMC gel spheres. Notably, changes were observed in the positions and intensities of the C1s, O1s, and S2p peaks following the adsorption of RhB dye. As illustrated in Fig. 8b, the binding energies of the C1s spectra included peaks at 284.8 eV (representative of C–C, C–H (aromatic)), 286.72 eV (C–O, C–*O*–C (carbonyl and ether)), and 288.78 eV (-COOH (carboxyl)). These binding energies shifted upon the adsorption of RhB, which was attributed to the interaction between the carboxyl groups on the surface of the gel spheres and the azo groups in the RhB dye [27]. Such a shift in binding energies indicated a chemical interaction between the adsorbent and the dye, providing insights into the nature of the adsorption mechanism at a molecular level. The core orbital peak area experienced an augmentation, a consequence of the formation of robust hydrogen bonds between the carboxyl (-COOH) group in the gel spheres and the azo (-N═N-), amine (–NH–), and amide (-NH_2) groups in RhB. This interaction altered the binding energy [51]. The O1s X-ray photoelectron spectroscopy (XPS) data, presented in Fig. 8c, showed that post-adsorption, the binding energies of C–O and C═O bonds decreased by 0.09 eV and 0.11 eV, respectively. Fig. 8d displayed the S2p XPS data. The binding energy associated with sulfate compounds [52] (RSO_4) was observed to decrease from 169.98 eV to 169.64 eV following RhB adsorption. Concurrently, the binding energy linked to the physisorbed species of sodium dodecyl sulfate (SDS) with LDHs [53] diminished by 0.25 eV from 168.7 eV. This shift indicated a transformation in the chemical environment surrounding the SDS, reflecting changes in its S2p electronic state. These alterations in binding energies and peak areas in the XPS spectra provided insights into the molecular interactions underpinning the adsorption process, highlighting the complex interplay of chemical forces during the adsorption of RhB onto the modified LDHs/SA/CMC gel spheres.

Drawing from the observed impact of pH on adsorption, coupled with data from FTIR and XPS, it was determined that the adsorption of RhB by modified LDHs/SA/CMC gel pellets predominantly occurred through electrostatic adsorption, hydrogen bonding, and hydrophobic interactions. This multifaceted adsorption mechanism highlights the complex interplay of forces at play, enabling the effective capture of RhB molecules by the gel spheres.

3.9. Desorption and regeneration experiment

As evidenced in Fig. 9, the adsorption efficiency of the modified LDHs/SA/CMC gel spheres for RhB exhibited a decline as the number of utilization cycles increased. Nevertheless, even after four cycles of usage, the modified LDHs/SA/CMC gel spheres maintained commendable adsorption performance for RhB. The adsorption capacity for RhB remained significant at 24.76 mg/g, and the removal rate consistently exceeded 82 %. The used spheres are shown in Fig. S2. After four cycles of the adsorption test, the removal ability of the spheres for RhB was still good, and its appearance did not change significantly. This resilience in adsorptive capability across multiple cycles underscores the robustness and potential reusability of the modified LDHs/SA/CMC gel spheres in practical applications.

3.10. Adsorption performance comparison

To substantiate the superior adsorptive properties of the modified LDHs/SA/CMC gel spheres, the comparative analysis with several previously reported adsorbents was conducted. As shown in Table 5, the adsorption capacity of LDHs gel spheres was improved compared to the modified LDHs (48.29 mg/g), and compared with other large particle size adsorbent materials which were easy to apply, the gel pellets also had good performance in adsorbing RhB. In addition, the gel spheres were simple to prepare, easy to use and recycle, which was expected to be applied to practical engineering.

4. Conclusion

In this study, SDS intercalation-modified MgAl-LDHs were synthesized via a co-precipitation method. Subsequently, these were crosslinked with SA and CMC to form modified LDHs/SA/CMC gel spheres. The adsorptive properties of these spheres towards RhB were investigated. Results indicated that the modified LDHs/SA/CMC gel spheres achieved adsorption equilibrium after 600 min at pH 5.0, with a removal rate of RhB reaching 91.49 % and a maximum adsorption capacity of 59.64 mg/g at 25 °C. The adsorption process of RhB onto the gel spheres was characterized as a spontaneous endothermic reaction, aligning with the pseudo-second-order kinetic model and Langmuir adsorption isotherm. Even after four utilization cycles, the RhB removal efficiency of the gel spheres remained above 80 %, highlighting their potential as valuable adsorbents. The primary mechanisms underlying the adsorption of RhB by the modified LDHs/SA/CMC gel spheres were identified as electrostatic adsorption, hydrogen bonding, and hydrophobic interactions.

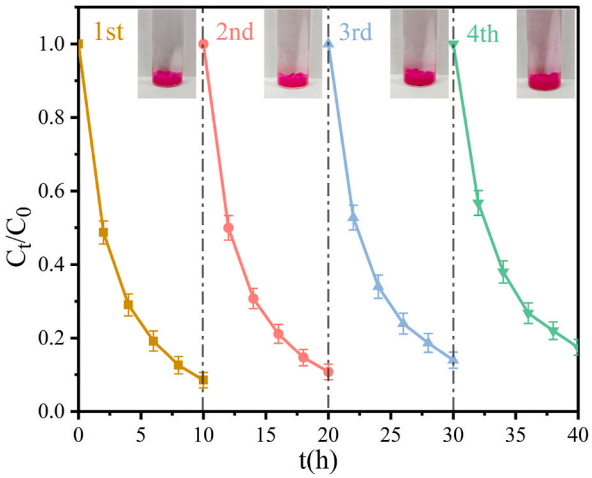

Fig. 9. Desorption and regeneration experiments of RhB by modified LDHs/SA/CMC gel spheres.

Table 5
Comparison of adsorption performance of different adsorbents for RhB.

Adsorbent	Morphological	q_m (mg/g)	Reference
Modified LDHs/SA/CMC gel spheres	sphere	59.64	This study
Modified LDHs	powder	48.29	[54]
P–N–GO hydrogel	lump	11.91	[55]
CMC-based composite hydrogel	lamellar	19.86	[56]
PPy hydrogel	sphere	22.60	[57]
ZIF-67 loaded activated carbon pellets	sphere	46.20	[58]
Bioconjugated graphene oxide hydrogel	lamellar	62.00	[59]

Data availability

Data will be made available on request.

CRediT authorship contribution statement

Siqi Chang: Writing – review & editing, Writing – original draft, Data curation. **Xiangling Zhang:** Writing – review & editing, Supervision, Methodology, Funding acquisition. **Chen Wang:** Writing – review & editing, Methodology. **Jing Bai:** Writing – review & editing, Validation, Conceptualization. **Xuhao Li:** Writing – review & editing, Validation, Conceptualization. **Wei Liang:** Validation, Formal analysis, Data curation. **Yajia Mao:** Validation, Formal analysis, Data curation. **Jixian Cai:** Validation, Formal analysis, Data curation. **Yifan Li:** Validation, Formal analysis, Data curation. **Yu Jiang:** Visualization, Formal analysis. **Zhouying Xu:** Validation, Formal analysis, Data curation.

Declaration of competing interest

The authors declare that they have no known competing financial interests or personal relationships that could have appeared to influence the work reported in this paper.

Acknowledgments

This work was funded by the National Natural Science Foundation of China (NO. 31670541).

Appendix A. Supplementary data

Supplementary data to this article can be found online at https://doi.org/10.1016/j.heliyon.2024.e30345.

References

[1] H.X. Zhou, A.J. Margenot, Y.K. Li, B.C. Si, T.F. Wang, Y.Y. Zhang, S.Y. Li, R. Bhattarai, Phosphorus pollution control using waste-based adsorbents: material synthesis, modification, and sustainability, Crit. Rev. Environ. Sci. Technol. 52 (2022) 2023–2059.
[2] O. Hamdaoui, Intensification of the sorption of Rhodamine B from aqueous phase by loquat seeds using ultrasound, Desalination 271 (2011) 279–286.
[3] A.A. Al-Gheethi, Q.M. Azhar, P.S. Kumar, A.A. Yusuf, A.K. Al-Buriahi, R. Mohamed, M.M. Al-shaibani, Sustainable approaches for removing Rhodamine B dye using agricultural waste adsorbents: a review, Chemosphere 287 (2022) 132080.
[4] S.A. Bhat, N. Rashid, M.A. Rather, S.A. Bhat, P.P. Ingole, M.A. Bhat, Highly efficient catalytic reductive degradation of Rhodamine-B over Palladium-reduced graphene oxide nanocomposite, Chem. Phys. Lett. 754 (2020) 137724.
[5] X.F. Ma, S.Y. Zhao, Z.W. Tian, G.G. Duan, H.Y. Pan, Y.Y. Yue, S.S. Li, S.J. Jian, W.S. Yang, K.M. Liu, S.J. He, S.H. Jiang, MOFs meet wood: reusable magnetic hydrophilic composites toward efficient water treatment with super-high dye adsorption capacity at high dye concentration, Chem. Eng. J. 446 (2022) 136851.
[6] L.R.S. Pinheiro, D.G. Gradissimo, L.P. Xavier, A.V. Santos, Degradation of azo dyes: bacterial potential for bioremediation, Sustainability 14 (2022) 1510.
[7] G.A. Ismail, H. Sakai, Review on effect of different type of dyes on advanced oxidation processes (AOPs) for textile color removal, Chemosphere 291 (2022) 132906.
[8] Y. Feng, Z.J. Zhang, Y.H. Zhao, L. Song, X.W. Wang, S.M. Yang, Y.Y. Long, C.H. Zhao, L.P. Qiu, Accelerated Rhodamine B removal by enlarged anode electric biological (EAEB) with electro-biological particle electrode (EPE) made from steel converter slag (SCS), Bioresour. Technol. 283 (2019) 1–9.
[9] M. Behera, J. Nayak, S. Banerjee, S. Chakrabortty, S.K. Tripathy, A review on the treatment of textile industry waste effluents towards the development of efficient mitigation strategy: an integrated system design approach, J. Environ. Chem. Eng. 9 (2021) 105277.
[10] G.L. Cao, R.P. Wang, Y. Ju, B.H. Jing, X.G. Duan, Z.M. Ao, J. Jiang, F.H. Li, S.H. Ho, Synchronous removal of emulsions and soluble organic contaminants via a microalgae-based membrane system: performance and mechanisms, Water Res. 206 (2021) 117741.
[11] H.N. Tran, C.C. Lin, H.P. Chao, Amino acids-intercalated Mg/Al layered double hydroxides as dual-electronic adsorbent for effective removal of cationic and oxyanionic metal ions, Separ. Purif. Technol. 192 (2018) 36–45.
[12] C.T. Vu, T.T. Wu, Magnetic porous NiLa-Layered double oxides (LDOs) with improved phosphate adsorption and antibacterial activity for treatment of secondary effluent, Water Res. 175 (2020) 115679.
[13] P. Zhang, S.D. Ouyang, P. Li, Y. Huang, R.L. Frost, Enhanced removal of ionic dyes by hierarchical organic three-dimensional layered double hydroxide prepared via soft-template synthesis with mechanism study, Chem. Eng. J. 360 (2019) 1137–1149.
[14] C.T. Gueho, V. Prevot, C. Forano, G. Renaudin, C. Mousty, F. Leroux, Tailoring hybrid layered double hydroxides for the development of innovative applications, Adv. Funct. Mater. 28 (2018) 1703868.
[15] F. Liu, Q. Yang, Q. Tang, Q. Peng, Y. Chen, Y. Huo, Q. Huang, Q. Zuo, N. Gao, L. Chen, Adsorption of RhB dye on soy protein isolate-based double network spheres: compromise between the removal efficiency and the mechanical strength, Chem. Eng. Res. Des. 193 (2023) 268–280.
[16] A. Chakraborty, H. Acharya, Facile synthesis of MgAl-layered double hydroxide supported metal organic framework nanocomposite for adsorptive removal of methyl orange dye, Colloid and Interface Science Communications 24 (2018) 35–39.
[17] S. Nouaa, R. Aziam, R. Benhiti, G. Carja, S. Iaich, M. Zerbet, M. Chiban, Synthesis of LDH/Alginate composite beads as a potential adsorbent for phosphate removal: kinetic and equilibrium studies, Chem. Pap. (2023) 6689–6705.
[18] H. Zhang, A.M. Omer, Z.H. Hu, L.Y. Yang, C. Ji, X.K. Ouyang, Fabrication of magnetic bentonite/carboxymethyl chitosan/sodium alginate hydrogel beads for Cu (II) adsorption, Int. J. Biol. Macromol. 135 (2019) 490–500.
[19] Z.L. Qing, L.J. Wang, X.Y. Liu, Z.W. Song, F. Qian, Y.H. Song, Simply synthesized sodium alginate/zirconium hydrogel as adsorbent for phosphate adsorption from aqueous solution: performance and mechanisms, Chemosphere 291 (2022) 133103.
[20] X.C. Zeng, G.H. Zhang, J. Wen, X.L. Li, J.F. Zhu, Z. Wu, Simultaneous removal of aqueous same ionic type heavy metals and dyes by a magnetic chitosan/polyethyleneimine embedded hydrophobic sodium alginate composite: performance, interaction and mechanism, Chemosphere 318 (2023) 137869.
[21] Z.H. Hu, A.M. Omer, X.K. Ouyang, D. Yu, Fabrication of carboxylated cellulose nanocrystal/sodium alginate hydrogel beads for adsorption of Pb(II) from aqueous solution, Int. J. Biol. Macromol. 108 (2018) 149–157.
[22] R. Ahmad, A. Mirza, Adsorption of Pb(II) and Cu(II) by Alginate-Au-Mica bionanocomposite: kinetic, isotherm and thermodynamic studies, Process Saf. Environ. Protect. 109 (2017) 1–10.
[23] C. Gao, X.L. Wang, Q.D. An, Z.Y. Xiao, S.R. Zhai, Synergistic preparation of modified alginate aerogel with melamine/chitosan for efficiently selective adsorption of lead ions, Carbohydr. Polym. 256 (2021) 117564.
[24] T. Gao, W. Wang, A. Wang, A pH-sensitive composite hydrogel based on sodium alginate and medical stone: synthesis, swelling, and heavy metal ions adsorption properties, Macromol. Res. 19 (2011) 739–748.
[25] M.A. Mohamed, Swelling characteristics and application of gamma-radiation on irradiated SBR-carboxymethlycellulose (CMC) blends, Arab. J. Chem. 5 (2012) 207–211.
[26] J.H. Bai, R. Wang, X.M. Wang, S.D. Liu, X.L. Wang, J.M. Ma, Z.H. Qin, T.F. Jiao, Biomineral calcium-ion-mediated conductive hydrogels with high stretchability and self-adhesiveness for sensitive iontronic sensors, Cell Reports Physical Science 2 (2021) 100623.
[27] C. Chen, E. He, W. Jia, S. Xia, L. Yu, Preparation of magnetic sodium alginate/sodium carboxymethylcellulose interpenetrating network gel spheres and use in superefficient adsorption of direct dyes in water, Int. J. Biol. Macromol. 253 (2023) 126985.
[28] H.X. Ren, Z.M. Gao, D.J. Wu, J.H. Jiang, Y.M. Sun, C.W. Luo, Efficient Pb(II) removal using sodium alginate-carboxymethyl cellulose gel beads: preparation, characterization, and adsorption mechanism, Carbohydr. Polym. 137 (2016) 402–409.
[29] S. Azizian, S. Eris, L.D. Wilson, Re-evaluation of the century-old Langmuir isotherm for modeling adsorption phenomena in solution, Chem. Phys. 513 (2018) 99–104.
[30] H. Yang, H. Hou, M. Yang, Z. Zhu, H. Fu, D. Zhang, Y. Luo, W. Yang, Engineering the S-scheme heterojunction between NiO microrods and MgAl-LDH nanoplates for efficient and selective photoreduction of CO_2 to CH_4, Chem. Eng. J. 474 (2023) 145813.
[31] H. Bera, S.G. Kandukuri, A.K. Nayak, S. Boddupalli, Alginate-sterculia gum gel-coated oil-entrapped alginate beads for gastroretentive risperidone delivery, Carbohydr. Polym. 120 (2015) 74–84.
[32] B.Y. Swamy, Y.S. Yun, In vitro release of metformin from iron (III) cross-linked alginate-carboxymethyl cellulose hydrogel beads, Int. J. Biol. Macromol. 77 (2015) 114–119.
[33] H. Ren, Z. Gao, D. Wu, J. Jiang, Y. Sun, C. Luo, Efficient Pb(II) removal using sodium alginate–carboxymethyl cellulose gel beads: preparation, characterization, and adsorption mechanism, Carbohydr. Polym. 137 (2016) 402–409.
[34] P. Zhang, G.R. Qian, Z.P. Xu, H.S. Shi, X.X. Ruan, J. Yang, R.L. Frost, Effective adsorption of sodium dodecylsulfate (SDS) by hydrocalumite (CaAl-LDH-Cl) induced by self-dissolution and re-precipitation mechanism, J. Colloid Interface Sci. 367 (2012) 264–271.
[35] P. Zhang, T.Q. Wang, G.R. Qian, D.S. Wu, R.L. Frost, Effective intercalation of sodium dodecylsulfate (SDS) into hydrocalumite: mechanism discussion via near-infrared and mid-infrared investigations, Spectrochim. Acta Mol. Biomol. Spectrosc. 149 (2015) 166–172.
[36] X.X. Ruan, S. Huang, H. Chen, G.R. Qian, Sorption of aqueous organic contaminants onto dodecyl sulfate intercalated magnesium iron layered double hydroxide, Appl. Clay Sci. 72 (2013) 96–103.
[37] M. Thommes, K. Kaneko, A.V. Neimark, J.P. Olivier, F. Rodriguez-Reinoso, J. Rouquerol, K.S.W. Sing, Physisorption of gases, with special reference to the evaluation of surface area and pore size distribution (IUPAC Technical Report), Pure Appl. Chem. 87 (2015) 1051–1069.
[38] T. Xu, S. An, C. Peng, J. Hu, H. Liu, Construction of large-pore crystalline covalent organic framework as high-performance adsorbent for rhodamine B dye removal, Ind. Eng. Chem. Res. 59 (2020) 8315–8322.
[39] C. Xiang, C. Wang, R.H. Guo, J.W. Lan, S.J. Lin, S.X. Jiang, X.X. Lai, Y. Zhang, H.Y. Xiao, Synthesis of carboxymethyl cellulose-reduced graphene oxide aerogel for efficient removal of organic liquids and dyes, J. Mater. Sci. 54 (2019) 1872–1883.
[40] K.G. Bhattacharyya, S. SenGupta, G.K. Sarma, Interactions of the dye, Rhodamine B with kaolinite and montmorillonite in water, Appl. Clay Sci. 99 (2014) 7–17.

[41] J.P. Simonin, On the comparison of pseudo-first order and pseudo-second order rate laws in the modeling of adsorption kinetics, Chem. Eng. J. 300 (2016) 254–263.
[42] L. Shang, X.Z. Dong, C.X. Liu, Z. Gong, Fast grid frequency and voltage control of battery energy storage system based on the amplitude-phase-locked-loop, IEEE Trans. Smart Grid 13 (2022) 941–953.
[43] J.P. Vareda, On validity, physical meaning, mechanism insights and regression of adsorption kinetic models, J. Mol. Liq. 376 (2023) 121416.
[44] T.Z. Shi, Z.F. Xie, X.L. Mo, Y.L. Feng, T. Peng, D.D. Song, Highly efficient adsorption of heavy metals and cationic dyes by smart functionalized sodium alginate hydrogels, Gels 8 (2022) 343.
[45] Y.Z. Niu, R.J. Qu, H. Chen, L. Mu, X.G. Liu, T. Wang, Y. Zhang, C.M. Sun, Synthesis of silica gel supported salicylaldehyde modified PAMAM dendrimers for the effective removal of Hg(II) from aqueous solution, J. Hazard Mater. 278 (2014) 267–278.
[46] Y. Tang, X. Zhang, X. Li, J. Bai, C. Yang, Y. Zhang, Z. Xu, X. Jin, Y. Jiang, Facile synthesis of magnetic ZnAl layered double hydroxides and efficient adsorption of malachite green and Congo red, Separ. Purif. Technol. 322 (2023) 124305.
[47] O. Amrhar, L. El Gana, M. Mobarak, Calculation of adsorption isotherms by statistical physics models: a review, Environ. Chem. Lett. 19 (2021) 4519–4547.
[48] W.L. Xu, S. Chen, Y.N. Zhu, X.X. Xiang, Y.Q. Bo, Z.M. Lin, H. Wu, H. Liu, Preparation of hyperelastic graphene/carboxymethyl cellulose composite aerogels by ambient pressure drying and its adsorption applications, J. Mater. Sci. 55 (2020) 10543–10557.
[49] P. Liu, M.G. Chen, C.G. Xiong, X.H. Cao, H. Wang, Flexible and highly sensitive graphene/carboxymethyl cellulose films for bending sensing, J. Mater. Sci. Mater. Electron. 31 (2020) 14118–14127.
[50] X.Y. Zhou, J.F. Wei, K. Liu, N.N. Liu, B. Zhou, Adsorption of bisphenol A based on synergy between hydrogen bonding and hydrophobic interaction, Langmuir 30 (2014) 13861–13868.
[51] X. Dong, Y.C. Lin, Y.Q. Ma, L. Zhao, N-contaning UiO-67 derived multifunctional hybrid materials as highly effective adsorbents for removal of red, Inorg. Chim. Acta. 510 (2020) 119748.
[52] L. Madec, J. Xia, R. Petibon, K.J. Nelson, J.P. Sun, I.G. Hill, J.R. Dahn, Effect of sulfate electrolyte additives on $LiNi_{1/3}Mn_{1/3}Co_{1/3}O_2$/graphite pouch cell lifetime: correlation between XPS surface studies and electrochemical test results, J. Phys. Chem. C 118 (2014) 29608–29622.
[53] N.S. Mirbagheri, S. Sabbaghi, A Ti-doped γ-Fe_2O_3/SDS nano-photocatalyst as an efficient adsorbent for removal of methylene blue from aqueous solutions, J. Environ. Manag. 213 (2018) 56–65.
[54] P. Zhang, S. Ouyang, P. Li, Y. Huang, R.L. Frost, Enhanced removal of ionic dyes by hierarchical organic three-dimensional layered double hydroxide prepared via soft-template synthesis with mechanism study, Chem. Eng. J. 360 (2019) 1137–1149.
[55] R. Wang, Q. Yu, Y. He, J. Bai, T. Jiao, L. Zhang, Z. Bai, J. Zhou, Q. Peng, Self-assembled polyelectrolyte-based composite hydrogels with enhanced stretchable and adsorption performances, J. Mol. Liq. 294 (2019) 111576.
[56] H. Zhao, Z.X. Liang, Z.Z. Gao, Facile preparation of floatable carboxymethyl cellulose-based composite hydrogel for efficient removal of organic dyes, Colloid and Interface Science Communications 49 (2022) 100637.
[57] T. Yao, W. Jia, X. Tong, Y. Feng, Y. Qi, X. Zhang, J. Wu, One-step preparation of nanobeads-based polypyrrole hydrogel by a reactive-template method and their applications in adsorption and catalysis, J. Colloid Interface Sci. 527 (2018) 214–221.
[58] Y. Li, X. Yan, X. Hu, R. Feng, M. Zhou, Trace pyrolyzed ZIF-67 loaded activated carbon pellets for enhanced adsorption and catalytic degradation of Rhodamine B in water, Chem. Eng. J. 375 (2019) 122003.
[59] K. Soleimani, Abbas D. Tehrani, M. Adeli, Bioconjugated graphene oxide hydrogel as an effective adsorbent for cationic dyes removal, Ecotoxicol. Environ. Saf. 147 (2018) 34–42.